Egypt. J. Chem. **Vol. 65**, No. 5 pp. 325 -335 (2022)

Egyptian Journal of Chemistry

http://ejchem.journals.ekb.eg/

Synthesis and investigation of green hydrogels for simultaneous removal of mercuric cations and methylene blue from aqueous solutions

Mohamed Keshawy[1*], Rasha S. Kamal[1] and Manar El-Sayed Abdel-raouf [1]

[1]Petroleum Applications Department, Egyptian Petroleum Research Institute, Cairo, Egypt

Abstract

A green composite comprised of guar gum (GG)/chitosan (CH) cross-linked with glutaraldehyde was prepared and then enforced with different weight ratios (1, 2, and 3%) of talc powder (TP) as inorganic support. This group of green sorbent materials was introduced to remove methylene blue and toxic heavy metal cation (Hg^{+2}) from aqueous solutions. The chemical modification was proved by the IR spectroscopy and the prepared hydrogels were investigated by X-ray diffraction (XRD) for their crystallinity. The thermal properties of the green sorbents were evaluated by the Thermal gravimetric analysis (TGA). Scanning electron microscopy (SEM) and Atomic force microscopy (AFM) were used to investigate the surface features and surface topography of the optimum adsorbent before and after adsorption respectively. Adsorption experiments were conducted as functions versus the contact time and temperature. Moreover, isothermal, thermodynamic adsorption, and kinetic theoretical constants were calculated. Results revealed that guar gum/chitosan grafted nanocomposite GG/CH/GA/T2 enhanced the removal of methylene blue (MB) up to (79%) and metal ion discharge (92.11%). The maximum cationic dye MB and Hg^{+2} ions adsorption efficiencies were reached at temperature (318 K). For both MB dye and Hg^{+2} ions, the pseudo-2nd -order model has successfully defined the adsorption kinetics and the Langmuir model could exactly explain adsorption isotherms for both Hg^{+2} and MB dye. Hg^{+2} and MB dye have recorded the maximum removal performance of 277.4 and 57.992 mg/g respectively on GG/CH/GA/T2 at 25 °C; indicating an efficient separation of adsorbent from aqueous solutions for both cationic dyes and toxic heavy metals.

Keywords: *Guar gum, chitosan, talc powder, magnetic nanoparticles, cationic dye, mercury.*

1. Introduction

Recently, composites based on green polymers and inorganic materials have been considered as a substitute for sorption applications (adsorbents and absorbents) [1–3]. Superabsorbents are able to hold immense amounts of water with respect to their original mass and retain them captured on their surface or entrapped within their interior voids [4,5]. Superabsorbents are usually applied in water retention applications such as health and agriculture [6–10]. There are many natural materials used in the field of wastewater remediation, such as chitosan/calcium alginate [11], starch [12,13], cyclodextrin [14] cellulose [15] and rosin [16]. Some petroleum-based polymers were also modified as sorbents for heavy metals such as polystyrene [17], and tyres [18]. The fabrication of natural polymers with inorganic materials with monometallic core (Fe3O4) or bimetallic core MFe2O4 (M = Co, Zn, Mn, Ni) was proved to enhance the mechanical properties and physical characteristics [19]. On the other hand, guar gum and chitosan are among the most abundant natural polymers [20]. The combination of these polymers in a composite formulation is highly favored due to their immunogenicity, hydrophilicity, biodegradability, and the readiness of hydrogel formation with various cross-linkers [21,22]. Modification of these polymers by crosslinking into hydrogels was proved as an efficient modification to improve their adsorption effectiveness to various kinds of pigments and poisonous heavy metals [23–25]. They may serve as an economic source of heavy metals by recovering the adsorbed metals. Methylene blue (MB, Figure 1) is one of the major contaminants in the environment caused by a wide range of coloring industries, such as cosmetics, leather, printing, textiles, food, and plastics [26,27].

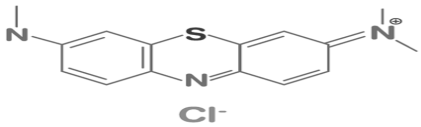

Figure 1: Structure of Methylene blue ($C_{16}H_{18}ClN_3S$)

It is responsible of many common side effects including headache, vomiting, confusion, shortness of breath, and high blood pressure. Other side effects include serotonin syndrome, red blood cell breakdown, and allergic reactions [28]. Also, some heavy metals such as lead, cadmium, copper, chromium pose a serious threat to the environment and human health [29]. Mercury has been classified among the most poisonous heavy metals due to its extreme toxicity even at a very low concentration and

*Corresponding author e-mail: elkeshawy2006@yahoo.com; (**Mohamed Keshawy**).

Receive Date: 12 October 2021, Revise Date: 02 November 2021, Accept Date: 07 November 2021

DOI: 10.21608/ejchem.2021.100722.4678

short exposure [30]. It is readily accumulated in the tissues and contribute to unlimited damage in human body [31]. On the other hand, super absorbent green hydrogels were extensively applied in different applications where water absorption or retention is important such as pharmaceutical and wastewater remediation [32–35]. Moreover, hydrogel composites were prepared by incorporation of different inorganic supports into the hydrogel matrix such as nanomagnetite [36], montmorillonite [37], graphene oxide [38] and silicates [39]. The objective of this work is to introduce superabsorbent green hydrogel matrix composed of guar gum /chitosan crosslinked with glutaraldehyde and fabricated with different weight ratios of Talc powder (di metal oxide inorganic core (Mg3Si4O10(OH)2) as sorbents for some toxic pollutants. The efficiency of the green composites is investigated versus different parameters.

2. Experimental

2.1. Materials:

Both commercial guar gum (GG) and chitosan (CH) from shrimp shells (with an average deacetylation degree of 87% were purchased from El-Nasr company for chemicals, Egypt. All other reagents: glutaraldehyde (GA), acetic acid, mercuric chloride and talc powder) were used as analytical grade and procured from Kima Aswan, Egypt. Methylene blue was obtained from Merck. CH (1%, w/v) was solubilized in 2% (v/v) acetic acid solution while GG (1%, w/v) was dissolved in distilled water.

2.2. Preparation of guar gum/chitosan-cl-glutaraldehyde:

:Hydrogels in this study were prepared as shown in Scheme 1. The weight ratios of the reactants (GG, CH, GA) were selected according to the optimized ratios mentioned by Sushmit et al [24] with slight modification. Briefly, A guar gum solution (1% (w/v)) solution was prepared and kept under mechanical stirring for 2 h at 1500 rpm and then it was acidified by addition of few drops of 98% concentrated sulfuric acid. In another beaker, 0.7 g of chitosan was added to 5% (v/v) acetic acid solution and the mixture was stirred for 4 h at room temperature, at 1500 rpm. Then, chitosan solution was added to the guar gum solution and the mixture was stirred for another two hours. To the guar gum/chitosan mixture, 10% of glutaraldehyde was added as crosslinking agent considering that Glutaraldehyde used was of 25% w/v solution in water. Thus, calculations of glutaraldehyde were made accordingly. The mixture was stirred for another 4 h at 40 ^{o}C. The obtained gels were dried in an oven at 70 °C till a constant weight then they were crushed into fine powder. All the prepared hydrogels were freeze-dried to keep their network structure.

2.3. Fabrication of the prepared hydrogel with inorganic supporter:

The modified hydrogels were prepared by addition of the desired weight ratio (1, 2 and 3%) of the talc powder with respect to the total weight of the guar gum and chitosan prior to the addition of the glutaraldehyde. Then the procedure was completed as per previous section. The codes and composition of the prepared green composites are tabulated in Table 1.

Table 1: Codes and composition of the green hydrogels

Code/composition	GG (gm)	CH (gm)	GA (gm)	TP(%)
GG/CH/GA	5	0.7	10	-----
GG/CH/GA/T1	5	0.7	10	1
GG/CH/GA/T2	5	0.7	10	2
GG/CH/GA/T3	5	0.7	10	3

2.4. Characterization:

Different characterization techniques were applied to ensure the chemical modification, to test the structural and thermal properties of the prepared hydrogel composites and to monitor their removal performance. These are;

- IR Spectroscopy: The IR spectra were recorded on a Perkin-Elmer 720 spectrophotometer with the resolution of 2 cm^{-1}, in the wavelength range of 400 to 4000 cm^{-1}.
- The surface morphology and particle size were studied on JEOL GSM 6510LV (SEM) scanning electron microscope.
- The surface topography was monitored via an AFM Flexaxiom nanosurf, C3000, dynamic mode, parabola fitting data filter.
- XRD patterns of the samples were obtained using a high-intensity Shimadzu diffractometer Cu Kα radiation (λ = 1.54065 Å) with a spectrum of 2θ ranging from 10° to 80°.
- The dynamic weight loss and thermal stability of the prepared samples were detected by thermogravimetric analysis that was carried out by a thermal analyzer (model Q600 SDT simultaneous DSC–TGA) with heating rate of 10 $^{\circ}$C/min under N_2 gas with the operating temperature of 30–800 $^{\circ}$C.

Atomic absorption Spectrophotometer model ZEEnit 700P(AAS)/ Germany/Analytikjena Co, was used to evaluate metal ions concentration in the solution, whilst UV–visible spectrophotometer model Unicam UV/vis, UK UV/vis spectrometer was utilized to detect the color intensity of the dye solution.

2.5. Comparative Analysis of removal performance:

A comparative analysis of adsorption performance between the prepared green hydrogels has been studied at initial concentration of 75 and 25 mg/L for both Hg^{+2} and MB, respectively, adsorbent dose of 0.1 g for both Hg^{+2} and MB, and maximum contact time 24 h.

2.6. Removal experiments:

The removal performance was monitored by batch experiments via the tea bag method as per our previous work [17]. Simply, the desired dose of the sorbent (0.2 g) was placed in a tea bag then the bag is immersed in a pollutant solution, and 1ml of the solution is drawn at the desired time. The initial experiments were performed at a constant temperature of 25 °C, with contact time 15, 30, 45, 60, 90, 120 minutes then after 24 hrs. The removal performance towards Hg^{+2} ions was assessed by atomic absorption spectrophotometer (AAS) while the elimination of MB was evaluated by UV–visible spectrophotometer for MB. The removal percentage of MB and hazardous heavy metal (Hg^{2+}) was estimated according to Eq. (1):

$$Removal\ percentage(\%) = \frac{(C_0 - C_e)}{C_0}\ x\ 100 \qquad (1)$$

where C_o is the initial concentration and C_e is the concentration at equilibrium.

The adsorption of MB and toxic (Hg^{+2}) ions was defined with the adsorption kinetics, the pseudo-1st-order, pseudo-2nd-order was utilized to present the information of adsorption process [40–43] in linear forms stated as:

$$\log(q_e - q_t) = \log(q_e) - \left(\frac{k_1}{2.303}\right)t \qquad (2)$$

$$\frac{t}{q_t} = \frac{1}{(k_2 q_e^2)} + \left(\frac{1}{q_e}\right)t \qquad (3)$$

where q_t and q_e are the concentrations of MB or toxic (Hg^{+2}) ions adsorbed at time t and equilibrium e, respectively; K_1 and K_2 are the pseudo-1st -order and pseudo-2nd order rate constants for the adsorption, respectively. The adsorbate can migrate from the solution phase to the surface of the adsorbent in a multi-step process. The steps may include film or external diffusion, pore diffusion, surface diffusion, and adsorption on the pore surface [44].

The adsorption process was evaluated by two isotherm models, Langmuir and Freundlich. The calculations are made according to the following mathematical relations [35]:

Langmuir model:

$$\frac{C_e}{q_e} = \frac{1}{K_L Q_L} + \frac{C_e}{Q_L} \qquad (4)$$

where K_L (mg/L) and Q_L (mg/g) are the Langmuir constants denoted to adsorption energy and sorption power respectively. Hence, q_e (mg/g) referred to the equilibrium adsorption capacity and C_e (mg/L) is defined as the equilibrium concentration.

Freundlich model:

$$logq_e = logK_f + \frac{1}{n} logC_e \qquad (5)$$

where the Freundlich constant K_f (mg/L) indicates the sorption capacity and the sorption intensity is expressed by n, which represents the heterogeneity function.

3. Results and discussion:

3.1. Mechanism of preparation of green hydrogels:

A general representation of the overall synthesis process is illustrated in scheme 1.

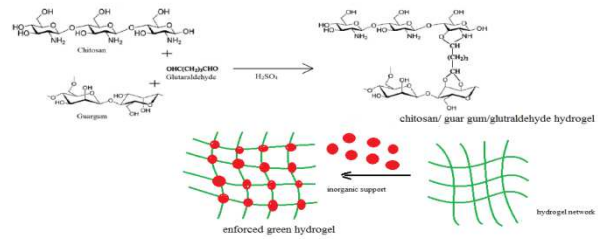

Scheme 1: Suggested mechanism for green hydrogel formation

The mechanism involves protonation of aldehyde group of the glutaraldehyde making it capable to react with the –OH group of guar gum and, -OH and $–NH_2$ groups of chitosan, forming water molecules and covalent linkages [36]. Sulfuric acid is added to guar gum solution not to the chitosan solution to avoid the spontaneous reaction with the $–NH_2$ groups of chitosan. The exact structure of the resulting network is not possible due to the presence of various forms of glutaraldehyde in solution (free aldehyde, mono- and dihydrated monomeric glutaraldehyde, monomeric and polymeric cyclic hemiacetals) [37,38]. However, glutaraldehyde has been used as a common cross-linker since it is cheap, readily available and highly soluble in aqueous solution. The inorganic material is incorporated within the gel matrix to enhance the mechanical properties during swelling and to increase the active surface area. The two specified materials have been proved as effective candidates for heavy metal removal [39,40] Talc powder $Mg_3[Si_4O_{10}](OH)_2$ is a hydrous silicate salt comprised of two major parts of oxides of silicon and magnesium It is one of the softest minerals ever known with specific surface area nearly about 4.3 $m^2\ g^{-1}$. The particle size distribution for talc powder used was between 30 and 350 nm and the mean particle size was 158 nm with a pore volume corresponding to 0.09 $m^2\ g^{-1}$ [41].

3.2. Characterization:

3.2.1. FT-IR description:

IR spectra of (a) CH, (b) GG, (c) GG/CH/GA and (d) GG/CH/GA/T2 are shown in Fig. 2I. It is apparent upon comparing these spectra, it is evident that new bands are formed at certain regions which confirms the linking of guar gum with chitosan. For instance, a peak of bending vibration of OH of guar gum and chitosan at 1630 cm^{-1} is decreased to a minimal indicating the cross-linking of glutaraldehyde via some hydroxyl groups. A small peak at 3660 cm^{-1} is indicative to the secondary amine group. Thus, it is evident from the FTIR spectra that the chitosan and guar gum are efficiently cross-linked by using glutaraldehyde as a crosslinker [42, 43]. The IR spectrum of talc powder shows a number of bands at wave numbers of 3680, 3445, 1044, 680 and 480 cm^{-1}

ascribed for different recognized functional groups such as the siloxane group (Si-O-Si) and the Si-O-Mg bond [45]. The occurrence of these peaks together with the peaks characterizing the functional groups of the crosslinked polymer prove the incorporation of the talc powder within the network structure. Our findings agree with Ossman et al. [40].

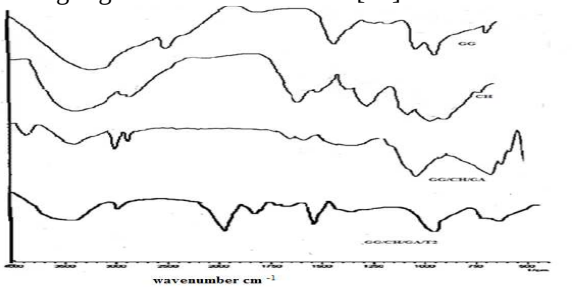

Figure 2I: The FT-IR spectra of GG, CH, GG/CH/GA, and GG/CH/GAT2

3.2.2. TGA analysis:

The thermogravimetric profiles for native guar gum and native chitosan are given in Figure [Fig. 2IIa]. Moreover, the thermograms of CH/GG/GA, and GG/CH/GA/T2 are illustrated in [Fig. 2IIb]. A comparison is held to evaluate the thermal behavior of the prepared green hydrogel composites and to monitor the effect of the inorganic material on the thermal stability of these hydrogels. Initially, the thermograms of both guar gum and chitosan [Fig. 2IIa] reveal low thermal stability [44,45]; about 80% of guar gum is degraded at 300 ^{o}C and nearly 70% of chitosan is tarnished at 320 ^{o}C. As observed in the TGA curve of the crosslinked hydrogel [Fig. 2IIb], there is a two-phases weight loss pattern. The first phase between 50 °C and 200 °C shows a weight reduction of about 20%. This may due to the loss of the adsorbed moisture. This phase is absent in the thermogram of the reinforced hydrogel, [GG/CH/GA/T2]. This proved that the reinforced crosslinked polymers were resistant to the absorption of moisture [41,42]. The second phase of weight loss starts at 400 °C and extends to 580 °C with about 70% weight loss owing to degradation of natural polymers (Guar gum and chitosan). This degradation pattern is of higher temperatures than the degradation temperatures of native polymers [46]. The degradation of (GG/CH/GA/T2) hydrogel takes place in two stage from 120–270, and 500–700 °C respectively. The first region could be attributed to the loss of some functional groups from the backbone of the crosslinked polymer such as hydroxyl and amine groups. These groups are known to form hydrogen bondings which strengthen the network. The second region might be due to the degradation of the crosslinked structure. Generally, it is observed that the incorporation of talc powder enhances the thermal stability of the product.

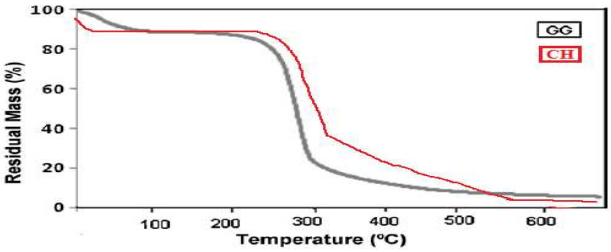

Figure 2IIa: Thermograms of native chitosan and native guar gum

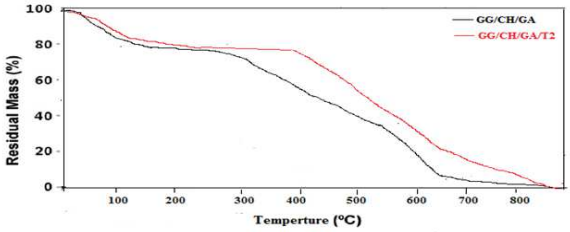

Figure 2IIb: Thermograms of GG/CH/GA and GG/CH/GAT2

3.2.3. XRD Patterns:

The chemical modification procedures could be proved by investigating the XRD patterns of the guar gum, chitosan, and talc powder before being formulated than comparing with the patterns of CH/GG/GA, and CH/GG/GAT2 . The XRD patterns of GG and CH are illustrated in Figure 2IIIa, whereas the XRD of talc powder, CH/GG/GA, and CH/GG/GAT2 are presented in Fig. 2IIIb. The scanning was conducted in the zone of 2θ from 0° to 70°. The diffraction pattern of native chitosan shows two peaks at 2θ=10^{o} and 20^{o} indicating the ordered crystalline structure of chitosan, which fully approve with the published report [47]. In contrast to chitosan, the XRD pattern of guar gum reveals an amorphous structure with low overall crystallinity.

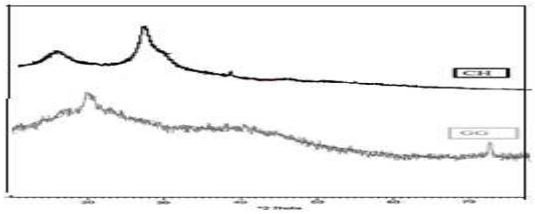

Figure 2IIIa: XRD patterns of GG and CH

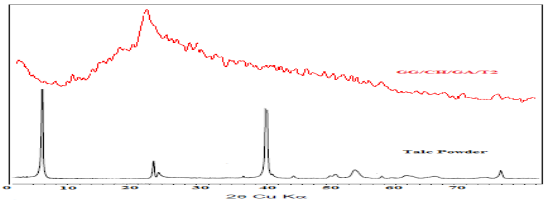

Figure 2IIIa: XRD patterns of Talc powder and GG/CH/GA/T2

The slight crystallinity is shown as low peak at 2θ=200 and it may be due to the intermolecular hydrogen bondings between the hydroxyl groups distributed throughout guar molecule [45]. On the other hand, the XRD pattern of talc powder reveals a strong crystalline structure with the peaks significant to the typical crystal strcture of talc, namely, at

$2\theta=7^{o}$, 25 ^{o} and 40^{o} [48,49]. When talc is incorporated within the network structure, it may bind some reactive hydroxyl and amine groups and loses its crystallinity. Therefore, the XRD of GG/CH/GA/T2, (Figure 2IIIb) depicts a semi-crystalline structure with a single wide peak at $2\theta=25^{o}$.

3.3. Electron Microscopy:

3.3.1. SEM investigation:

SEM is used to investigate the surface morphology of the hydrogel with and without inorganic supports. The SEM images of GG/CH/GA, and GG/CH/GAT2 are given in Figure IVa and IVb respectively. The SEM image of GG/CH/GA reveals a condensed flakes structure with distinct crosslinked points. On the other hand, the SEM of GG/CH/GAT2 shows the distributed talc particles within the hydrogel matrix.

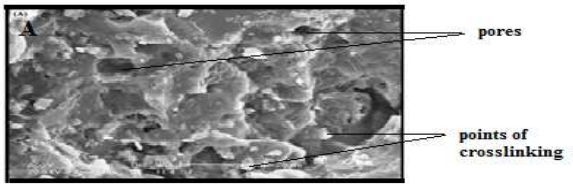

Figure IVa: SEM of GG/CH/GA

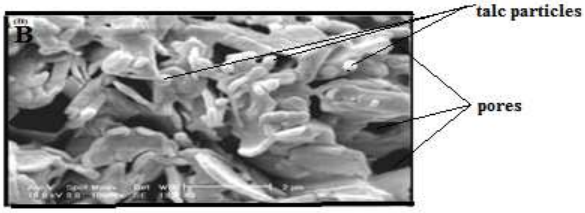

Figure IVb: SEM of GG/CH/GA/T2

3.3.2. AFM study: Surface characterization and roughness measurements:

The AFM was proved as an effective tool for investigating the hydrogels before and after the removal process by monitoring the surface topography and detect the incident changes due to the adsorbed species. In this regard, we applied an advanced AFM with wide Z and XY ranges to confirm the chemical modification process and monitor the swelling progression via the non-contact, dynamic mode. This was achieved by inspecting the following AFM outputs:

- The topography of the sample,
- The height represented by the Z-axis to measure the difference between the maximum point above the surface and the minimum point below the surface to describe the porous structure, and,

In this regard, the eight samples were investigated by the AFM, the images are illustrated in Figure V and the data elucidated from the AFM are given in Table 3. They include dry gels (gels without adsorbed species) and wet gels (loaded with either Hg^{+2} or MB).

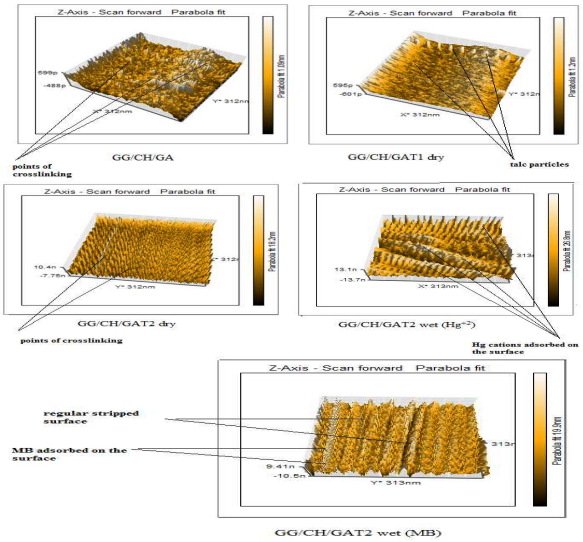

Figure V: The AFM images of some green hydrogels

These samples were carefully selected to confirm the data obtained from removal experiments and to reflect effect of the following variables on both the topography and the roughness:

- Weight percentage of the inorganic material.
- Type of adsorbate.

Table 3: AFM data for selected samples

No.	Sample	Height	Scale	Data analysis
1	GG/CH/GA	1.09 nm	312x312 nm	parabola
2	GG/CH/GAT1 dry	1.20 nm	312x312 nm	parabola
3	GG/CH/GAT2 dry	18.2 nm	312x312 nm	parabola
4	GG/CH/GAT2 wet (Hg^{+2})	26.8 nm	312x312 nm	parabola
5	GG/CH/GAT2 wet (MB)	19.9 n	312x312 nm	parabola

By investigating the tabulated AFM data, the following observations can be elucidated:

- The height increased by adding the inorganic material within the gel matrix, for instance, the height order for GG/CH/GA, GG/CH/GAT1 dry and GG/CH/GAT2 dry is 1.09 nm, 1.2 nm and 18.2 respectively.
- The topography and surface features are highly affected by the adsorption process. Moreover, the adsorbed species can be seen clearly on the surface of the hydrogel.
- The change in height goes parallel to the adsorption capability of the hydrogels. For instance, the tendency of GG/CH/GAT2 towards mercuric cation is higher than its tendency towards methylene blue. Therefore, the height of the gel adsorbed Hg^{+2} is 26.8 nm while it is 19.9 nm when it contains methylene blue.

GG/CH/GAT2 is the most active adsorbent versus both Hg^{+2} and methylene blue dye. This may be explained by its height measurements which reveals average pore size suitable for maximum removal.

3.4. Adsorption performance and mechanism:

3.4.1. Comparative Analysis of Adsorption Performance:

Figure VI shows a comparative investigation of adsorption performance between enforced and neat hydrogels toward the removal of $Hg^{+2}$and MB at the initial concentration of 75 and 25 mg/L for both Hg^{+2} and MB, respectively, and the adsorbent dose of 0.1 g for both Hg^{+2} and MB, for 24 h and at 25 °C. Results in Fig. VIa showed that the maximum removal effeciency for both Hg^{+2} and MB was attained by GG/CH/GA/T2 (92.11% and 79% for both Hg^{+2} and MB respectively). This finding agrees with all the previous findings elucidated from the XRD data considering the crystallinity of the enforced hydrogels and the AFM measurements regarding the heights of the hydrogels loaded with the removed species. This observation can be explained on the basis of the effect of talc powder on the network formation and the elasticity of the resulted network.

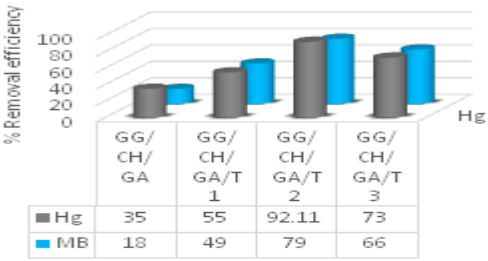

Figure VIa: Comparative analysis of adsorption performance between different green hydrogels toward the removal of Hg^{2+} and MB at initial concentration of 75 and 25 mg/L for both Hg^{2+} and MB, respectively, and adsorbent dose of 0.1 g for both Hg^{2+} and MB, respectively.

3.4.2. The Mechanism and kinetics of Adsorption:

The adsorption rate can be estimated by applying the pseudo-1st and pseudo-2nd-order kinetic designs. This correlation is illustrated in Figures VIb and VIc for removal of Hg^{+2} and MB respectively.

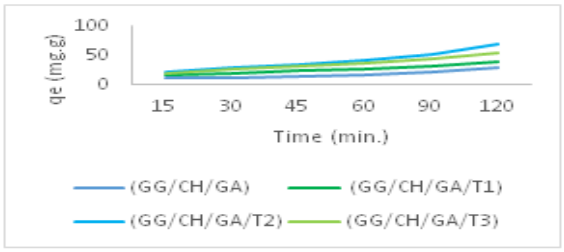

Figure VIb: Rate of adsorption of Hg^{+2}

Furthermore, Table 4 offers a description of the outcomes and obtained data. From the kinetic parameters, the pseudo-1st-order model envisages poor correlation coefficient values R^2 values: ranges from 0.5272 to 0.6281 for Hg^{+2} and from 0.5098 to 0.6097 for MB.

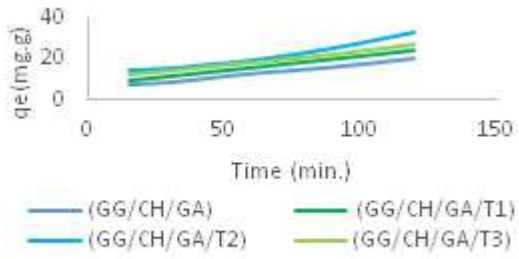

Figure VIc: Rate of adsorption of MB

Table 4: Kinetic parameters of the pseudo-1st and 2nd-order models for the adsorption of Hg^{2+} and MB onto neat and enforced GG/CH/GA hydrogels at pH=7 temperature at 25°C)

Hydrogel	Adsorbate	Kinetic model	Kinetic constants				
			R^2	$K_1(min^{-1})$	$q_{e,cal}$(mg/g)	K_2(g/mg min)	$q_{e,cal}$(mg/g)
GG/CH/GA	Hg^{+2}	Pseudo-1st order	0.5272	0.0064	5.7763		
		Pseudo-2nd order	0.9834			0.004567	7.47
	MB	Pseudo-1st order	0.5098	0.0059	3.4455		
		Pseudo-2nd order	0.9812			0.003078	4.78
GG/CH/GA/T1	Hg^{+2}	Pseudo-1st order	0.5286	0.0067	5.8256		
		Pseudo-2nd order	0.9857			0.004571	7.89
	MB	Pseudo-1st order	0.5438	0.0062	3.2319		
		Pseudo-2nd order	0.9873			0.003129	4.89
GG/CH/GA/T2	Hg^{+2}	Pseudo-1st order	0.6281	0.0073	5.9015		
		Pseudo-2nd order	0.9894			0.005641	7.94
	MB	Pseudo-1st order	0.5908	0.0079	3.7802		
		Pseudo-2nd order	0.9914			0.004709	5.66
GG/CH/GA/T3	Hg^{+2}	Pseudo-1st order	0.6137	0.0077	5.8842		
		Pseudo-2nd order	0.9943			0.005482	7.85
	MB	Pseudo-1st order	0.6097	0.0075	3.6817		
		Pseudo-2nd order	0.9925			0.004753	5.43

This assumed that the 1st-order pseudo models can not be used for explaining adsorption behavior, and no physical interaction was possible on the adsorbent surface between Hg^{+2} and MB ions and the functional groups of the polymer chains constituting the network structure. On the other hand, the improved correlation coefficients, R^2 (ranges between 0.9834 - 0.9983 for Hg^{+2} and from 0.9812 to 0.9943 for MB) suggested that the adsorption of both species on the green networks followed a kinetic model with a pseudo-2nd-order via chemical interaction between Hg^{+2} and MB and the functionalities of the adsorbate surface through the mutual or electron exchange or formation of chelate structure between sorbing and sorbed species [17,19,29]. The relationships depict also that the rate of diffusion increases by time and the effectiveness of the prepared hydrogels towards Hg^{+2} is more predominant than towards MB which may be due to the stability of the chelate structure between Hg^{+2} and the abundant functional groups found in the green polymers [50]. As it was proved by all the obtained data that GG/CH/GA/T2 showed the superlative performance, more investigation will be carried out to explore the isothermic parameters of adsorption by applying Langmuir and Freundlich equations, the data are given in Table 5. The first and second order kinetic isotherms of GG/CH/GA/T2 are given in Figure VII.

Table 5: Langmuir and Freundlich isothermic adsorption parameters for the Hg^{2+} and MB onto GG/CH/GA/T2, [equilibrium time of 24 h and temperatures of 25 °C, 35 °C, and 45 °C]

Adsorbate	Isotherm model	T(K)	Isotherm constants				
			R^2	Q_{max}(mg/g)	K_L (mg.L)	K_F(mg.L)	N
Hg^{2+}	Langmuir	298	0.8932	277.4	0.06604		
		308	0.9125	318.8	0.06718		
		318	0.9034	356.7	0.06859		
	Freundlich	298	0.9275			17.56	1.431
		308	0.9107			17.98	1.523
		318	0.9324			17.31	1.554
MB	Langmuir	298	0.0782	57.992	0.00205		
		308	0.0791	114.07	0.00247		
		318	0.8022	133.85	0.00311		
	Freundlich	298	0.8120			27.89	0.902
		308	0.8254			28.57	0.915
		318	0.8298			29.45	0.944

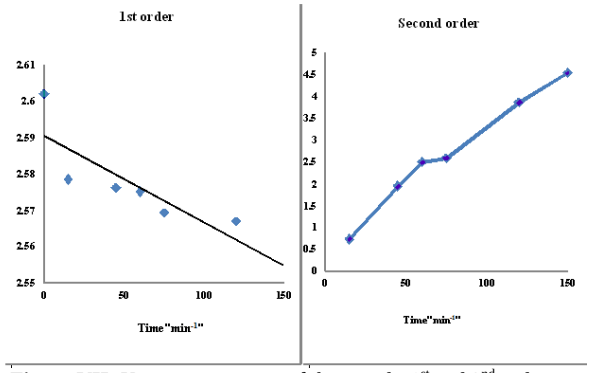

Figure VII: Kinetic parameters of the pseudo-1st and 2nd-order models for the adsorption of Hg^{2+} of GG/CH/GA/T2

The Langmuir pattern indicates the homogeneity of the monolayer that covers the adsorbate surface with clear linking points, equal energy of sorption, and homogeneous distribution of adsorbed molecules. On the other hand, the Freundlich isotherm is an indication for an adsorption process that takes place on heterogeneous substrates and the adsorber capacity is associated with a balanced adsorbent concentration The fitting of the Langmuir equations of Hg^{+2} and MB adsorption by GG/CH/GA/T2 at different temperatures are shown in Fig. VIII a and b. Also, their constant values are shown in Table 4 along with correlation factors (R^2). The highest uptakes for Hg^{+2} and MB were 277.4 and 57.992 mg/g respectively on GG/CH/GA/T2 at 25 °C. These values increase exponentially by raising the temperature from 25 to 35 °C. The calculated values of KL for adsorption of mercury cations and toxic MB on adsorbent indicate revealed a stronger depiction of the experimental findings by Langmuir model for both species. The observed rise of KL with an elevation of temperature may be referred to several assumptions such as an improvement in bond stability formed between the adsorbed materials and the surface of the sorbent and due to the increase in pore volume of the network structure.

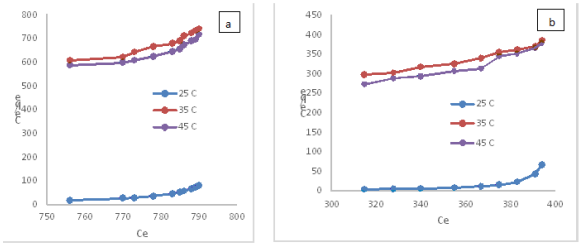

Fig. VIII: The fitting of the Langmuir quations for a- Hg^{+2} and b- MB adsorption by GG/CH/GA/T2 at different temperatures

3.4.3. Comparison of Hg^{+2} Ion and MB Adsorption Capacity on GG/CH/GA/T hydrogels:

Table 6 lists the adsorption capacity of Hg^{+2} cation and MB by different other adsorbents mentioned in other works, along with the results of the present study[51–57].

Table 6: Comparison of Hg^{2+}ion and MB adsorption capacity on GG/CH/GA/T2 with other adsorbents

Adsorbent	Adsorption capacity (mg/g)	References
MB		
alginate-g-PAMPS/$NiFe_2O_4$	22.81	[19]
betacyclodextrin-grafted-alginate	11.33	[51]
modified gum arabic, polyacrylate, and polyacrylamide	48	[52]
Cellulose-Based Superadsorbent Hydrogels	21.97	[53]
Clay	58.2	[54]
Superabsorbent hydrogel formed by modified gum arabic, polyacrylate, and polyacrylamide	48	[52]
Guar gum/chitosan/GA/Talc powder	57.992	The present study
Hg^{2+}		
alginate-g-PAMPS/$NiFe_2O_4$	275.5	[19]
Chitosan-graft-polyacrylamide semi-interpenetrating polymer network (IPN) superabsorbent hydrogel	2001.8	[55]
Chitosan-g-Poly(acrylic acid)/Attapulgite Hydrogel Composite	785.20, 679.63, and 541.06 according to Attapulgite content	[56]
thiourea-modified magnetic chitosan microspheres	625.2	[57]
Guar gum/chitosan/GA/Talc powder	277.4	The present study

The data indicate that the synthesized enforced green hydrogel (in the current study) has a remarkable adsorption capacity compared to many adsorbents. Moreover, the removal data confirm that the advanced green hydrogels can be considered as a promising and efficient sorbents for the simultaneous removal of Hg^{+2} ions and MB from aqueous solution.

Conclusion

The present work deals with removal of two types of potent pollutants (Hg^{+2} ions and MB) by introducing

green advanced hydrogel materials. The hydrogels are based on guar gum/chitosan crosslinked with glutaraldehyde and reinforced with different weight ratios of talc powder. The AFM was used to monitor the changes in the surface topography associating the changes in the network composition and also to verify the sorption process. The adsorption isotherms on the optimum composition GG/CH/GA/T1 were discussed. The adsorption kinetics was well depicted by the pseudo-2nd order design and the Langmuir model defined isothermic adsorption process for Hg^{+2} and MB dye adsorption. The optimal adsorption capacity was 277.4 and 57.992 mg/g respectively on GG/CH/GA/T2 at 25 °C, which increase by raising the temperature of the aqueous medium. The synthesized green hydrogels were proved as promising and efficient candidates for the simultaneous removal of Hg^{+2} ions and MB.

Conflicts of interest

There are no conflicts to declare.

References

[1] A. El-Kafrawy, S. El-Saeed, R. Farag, H. El-Saied, M.E.-S. Abdel-Raouf, Adsorbents based on natural polymers for removal of some heavy metals from aqueous solution, Egypt. J. Pet. 26 (207AD) 23–32. https://www.sciencedirect.com/science/article/pii/S1110062115301239 (accessed October 11, 2021).

[2] T. Hillie, M. Hlophe, Nanotechnology and the challenge of clean water, Nat. Nnotechnology. 2 (2007) 663–664. https://www.nature.com/articles/nnano.2007.350 (accessed October 11, 2021).

[3] S. V. Vassilev, D. Baxter, L.K. Andersen, C.G. Vassileva, An overview of the composition and application of biomass ash. Part 1. Phase–mineral and chemical composition and classification, Fuel. 105 (2013) 40–76. https://doi.org/10.1016/J.FUEL.2012.09.041.

[4] Manar El-Sayed Abdel-Raouf, A. Abdul-Raheim, Removal of Heavy Metals from Industrial Waste Water by Biomass-Based Materials: A Review, J. Pollut. Eff. Control. 5 (2017) 1. https://doi.org/10.4172/2375-4397.1000180.

[5] M. Raouf, N. Maysour, R.K. Farag., Wastewater treatment methodologies, review article, Int. J. Environ. Agric. Sci. 3 (2019) 1–18. https://www.researchgate.net/profile/Manar-El-Sayed-Abdel-Raouf/publication/332183222_Wastewater_Treatment_Methodologies_Review_Article/links/5ca526a592851c8e64b0f197/Wastewater-Treatment-Methodologies-Review-Article.pdf (accessed October 11, 2021).

[6] N. Thombare, S. Mishra, M. Siddiqui, U. Jha, D. Singh, G.R. & Mahajan, Design and development of guar gum based novel, superabsorbent and moisture retaining hydrogels for agricultural applications, Carbohydr. Polym. 185 (2018) 169–178. https://www.sciencedirect.com/science/article/pii/S0144861718300183 (accessed October 11, 2021).

[7] K. Chandrika, A. Singh, D.J. Sarkar, A. Rathore, A. & Kumar, pH□sensitive crosslinked guar gum□based superabsorbent hydrogels: Swelling response in simulated environments and water retention behavior in plant growth , J. Appl. Polym. Sci. 131 (2014) 41060. https://doi.org/10.1002/app.41060.

[8] S. Wang, H. Sun, H. Ang, M. Tadé, Adsorptive remediation of environmental pollutants using novel graphene-based nanomaterials, Chem. Eng. Journal 226 . 347–336 (2013). https://www.sciencedirect.com/science/article/pii/S1385894713005482 (accessed October 11, 2021).

[9] C. Chang, B. Duan, J. Cai, L. Zhang, Superabsorbent hydrogels based on cellulose for smart swelling and controllable delivery, Eur. Polym. J. 46 (2010) 92–100. https://www.sciencedirect.com/science/article/pii/S0014305709001864 (accessed October 11, 2021).

[10] T. Hussain, M. Ansari, N.M. Ranjha, I.U. Khan, Y. Shahzad, Chemically cross-Linked poly(acrylic- Co -Vinylsulfonic) acid hydrogel for the delivery of isosorbide mononitrate, Sci. World J. 2013 (2013) 1–9. https://doi.org/10.1155/2013/340737.

[11] Y. Vijaya, S.R. Popuri, V.M. Boddu, A. Krishnaiah, Modified chitosan and calcium alginate biopolymer sorbents for removal of nickel (II) through adsorption, Carbohydr. Polym. 72 (2008) 261–271. https://doi.org/10.1016/J.CARBPOL.2007.08.010.

[12] S. Sugashini, K.M.S. Begum., Column adsorption studies for the removal of Cr(VI) ions by ethylamine modified chitosan carbonized rice husk composite beads with modelling and optimization, J. Chem. (2013). https://doi.org/10.1155/2013/460971.

[13] A.R.M. Abdul-Raheim, M. El-Saeed Shimaa, R.K. Farag, E. Abdel-Raouf Manar, Low Cost Biosorbents Based On Modified Starch

Iron Oxide Nanocomposites For Selective Removal Of Some Heavy Metals From Aqueous Solutions: Polymer recycling View project oil spill View project Low cost biosorbents based on modified starch iron oxide nanoc, Adv. Mater. Lett. Adv. 7 (2016) 402–409. https://doi.org/10.5185/amlett.2016.6061.

[14] X. Zhang, H. Li, M. Cao, L. Shi, C. Chen, Adsorption of Basic Dyes on β-Cyclodextrin Functionalized Poly (Styrene-Alt-Maleic Anhydride), Sep. Sci. Technol. 50 (2015) 947–957. https://doi.org/10.1080/01496395.2014.978461.

[15] Y. Zhou, M. Zhang, X. Hu, X. Wang, J. Niu, T. Ma, Adsorption of cationic dyes on a cellulose-based multicarboxyl adsorbent, J. Chem. Eng. Data. 58 (2013) 413–421. https://doi.org/10.1021/JE301140C.

[16] Manar El-Sayed Abdel-Raouf and A. Abdul-Raheim, Rosin: Chemistry, Derivatives, and Applications: a review, BAOJ Chem 2018, 4 1, 4 039. 4 (2018) 4–39.

[17] M. Keshawy, A.R. Mahmoud, M.E.S. Abdel-Raouf, Polystyrene-based magnetic hydrogels for elimination of some toxic metal cations from aqueous solutions, Environ. Sci. Pollut. Res. 27 (2020) 26982–26997. https://doi.org/10.1007/S11356-020-08340-Z.

[18] E.L.K. Mui, D.C.K. Ko, G. McKay, Production of active carbons from waste tyres—a review, Carbon N. Y. 42 (2004) 2789–2805. https://doi.org/10.1016/J.CARBON.2004.06.023.

[19] H. El-saied, E. Motawea, Optimization and Adsorption Behavior of Nanostructured NiFe2O4/Poly AMPS Grafted Biopolymer, J. Polym. Environ. 28 (2020) 2335–2351. https://doi.org/10.1007/s10924-020-01774-z.

[20] S. Rithe, P. Kadam, S. Mhaske, Preparation and analysis of novel hydrogels prepared from the blend of guar gum and chitosan: Cross-linked with glutaraldehyde, Adv Mater Sci Eng. 1 (2014). https://www.academia.edu/download/64839337/1214msej01.pdf (accessed October 11, 2021).

[21] C. Xiao, J. Zhang, Z. Zhang, L. Zhang, Study of blend films from chitosan and hydroxypropyl guar gum, J. Appl. Polym. Sci. 90 (2003) 1991–1995. https://doi.org/10.1002/APP.12766.

[22] A.J. Sami, M. Khalid, T. Jamil, S. Aftab, Sermad, A. Mangat, A.R. Shakoori, S. Iqbal, Formulation of novel chitosan guargum based hydrogels for sustained drug release of paracetamol, Int. J. Biol. Macromol. 108 (2018) 324–332. https://www.sciencedirect.com/science/article/pii/S014181301732264X (accessed October 11, 2021).

[23] M. Vakili, M. Rafatullah, B. Salamatinia, A.Z. Abdullah, M.H. Ibrahim, ... & Tan, K. B., P. Amouzgar, Application of chitosan and its derivatives as adsorbents for dye removal from water and wastewater: A review, Carbohydr. Polym. 113 (2014) 115–130. https://www.sciencedirect.com/science/article/pii/S0144861714006729 (accessed October 11, 2021).

[24] B. Xu, H. Zheng, H. Zhou, Y. Wang, K. Luo, Z. C, P. Y, Z. X, Adsorptive removal of anionic dyes by chitosan-based magnetic microspheres with pH-responsive properties, J. Mol. Liq. 256 (2018) 424–432. https://www.sciencedirect.com/science/article/pii/S0167732217358919 (accessed October 11, 2021).

[25] L. Dai, Y. Wang, Z. Li, X. Wang, C. Duan, W. Zhao, A multifunctional self-crosslinked chitosan/cationic guar gum composite hydrogel and its versatile uses in phosphate-containing water treatment and energy , Carbohydr. Polym. 244 (2020) 116472. https://www.sciencedirect.com/science/article/pii/S0144861720306469 (accessed October 11, 2021).

[26] S. Dawood, T. Sen, Review on dye removal from its aqueous solution into alternative cost effective and non-conventional adsorbents, J. Chem. Process Eng. 104 (2014) 1–11. https://espace.curtin.edu.au/handle/20.500.11937/48131 (accessed October 11, 2021).

[27] Y. Li, W. Nie, P. Chen, Y. Zhou, Preparation and characterization of sulfonated poly (styrene-alt-maleic anhydride) and its selective removal of cationic dyes, Colloids Surfaces A Physicochem. Eng. Asp. 499 (2016) 46–53. https://www.sciencedirect.com/science/article/pii/S0927775716302345 (accessed October 11, 2021).

[28] P. Ken Gillman, Review: CNS toxicity involving methylene blue: The exemplar for understanding and predicting drug interactions that precipitate serotonin toxicity, J. Psychopharmacol. 25 (2011) 429–436. https://doi.org/10.1177/0269881109359098.

[29] H.A.A. El-saied, E.M. El-Fawal, Green superabsorbent nanocomposite hydrogels for high-efficiency adsorption and photo-degradation/reduction of toxic pollutants from waste water, Polym. Test. 97 (2021)

107134. https://www.sciencedirect.com/science/article/pii/S0142941821000842 (accessed October 11, 2021).

[30] K.M. Rice, E.M. Walker, M. Wu, C. Gillette, E.R. Blough, Environmental mercury and its toxic effects, J. Prev. Med. Public Heal. 47 (2014) 74–83. https://doi.org/10.3961/JPMPH.2014.47.2.74.

[31] R.A. Bernhoft, Mercury toxicity and treatment: a review of the literature, Mercur. Toxic. Treat. a Rev. Lit. J. Environ. Public Heal. (2012). https://www.hindawi.com/journals/jeph/2012/460508/ (accessed October 11, 2021).

[32] R. Hamilton, Tarascon Pocket Pharmacopoeia 2016 Deluxe Lab-Coat Edition2016 ‘. (n.d.). https://books.google.com/books?hl=ar&lr=&id=YISkDAAAQBAJ&oi=fnd&pg=PP1&dq=Hamilton,+Richart+(2015).+Tarascon+Pocket+Pharmacopoeia+2015+Deluxe+Lab-Coat+Edition.+Jones+%26+Bartlett+Learning.+p.+471.+ISBN+9781284057560.&ots=IgeJcNiF0Z&sig=IiKCL24FLbqnglj0Lv3 (accessed October 11, 2021).

[33] G. Bardajee, Z. Hooshyar, M. Asli, F. Shahidi, N. Dianatnejad, Synthesis of a novel supermagnetic iron oxide nanocomposite hydrogel based on graft copolymerization of poly ((2-dimethylamino) ethyl methacrylate) onto , Mater. Sci. Eng. 36 (2014) 277–286. https://www.sciencedirect.com/science/article/pii/S0928493113006358 (accessed October 11, 2021).

[34] H. Tang, H. Chen, B. Duan, A. Lu, L. Zhang, Swelling behaviors of superabsorbent chitin/carboxymethylcellulose hydrogels, J. Mater. Sci. 49 (2014) 2235–2242. https://doi.org/10.1007/S10853-013-7918-0.

[35] G.R. Bardajee, Z. Hooshyar, A novel biocompatible magnetic iron oxide nanoparticles/hydrogel based on poly (acrylic acid) grafted onto starch for controlled drug release, J. Polym. Res. 20 (2013) 298. https://doi.org/10.1007/S10965-013-0298-Y.

[36] C. Sandolo, P. Matricardi, F. Alhaique, T Coviello, Effect of temperature and cross-linking density on rheology of chemical cross-linked guar gum at the gel point, Food Hydrocoll. 23 (2009) 210–220. https://www.sciencedirect.com/science/article/pii/S0268005X08000040 (accessed October 11, 2021).

[37] J.I. Kawahara, T. Ohmori, T. Ohkubo, S. Hattori, M. & Kawamura, The structure of glutaraldehyde in aqueous solution determined by ultraviolet absorption and light scattering, Anal. Biochem. 201 (1992) 94–98. https://www.sciencedirect.com/science/article/pii/000326979290178A (accessed October 11, 2021).

[38] E. Whipple, M. Ruta, Structure of aqueous glutaraldehyde, J. Org. Chem. 39 (1974) 1666–1668. https://doi.org/10.1021/jo00925a015.

[39] H.A. El-saied, A.M. Shahr El-Din, B.A. Masry, A.M. Ibrahim, A Promising Superabsorbent Nanocomposite Based on Grafting Biopolymer/Nanomagnetite for Capture of 134Cs, 85Sr and 60Co Radionuclides, J. Polym. Environ. 28 (2020) 1749–1765. https://doi.org/10.1007/S10924-020-01720-Z.

[40] M. Ossman, M. Mansour, M. Fattah, N. Taha, Y. & Kiros, Peanut shells and talc powder for removal of hexavalent chromium from aqueous solutions, Bulg. Chem. Commun. 46 (2014) 629–639. https://www.researchgate.net/profile/Mona-Ossman-2/publication/269279024_Peanut_shells_and_talc_powder_for_removal_of_hexavalent_chromium_from_aqueous_solutions/links/5486163d0cf2ef34478bf433/Peanut-shells-and-talc-powder-for-removal-of-hexavalent-chromiu (accessed October 11, 2021).

[41] I.L. Lagadic, M.K. Mitchell, B.D. Payne, Highly effective adsorption of heavy metal ions by a thiol-functionalized magnesium phyllosilicate clay, Environ. Sci. Technol. 35 (2001) 984–990. https://doi.org/10.1021/ES001526M.

[42] S. Rithe, P. Kadam, S.M. Eng, Preparation and analysis of novel hydrogels prepared from the blend of guar gum and chitosan: Cross-linked with glutaraldehyde, Adv Mater Sci Eng. 1 (2014). https://www.academia.edu/download/64839337/1214msej01.pdf (accessed October 11, 2021).

[43] Y. Huang, J. Lu, C. Xiao, Thermal and mechanical properties of cationic guar gum/poly (acrylic acid) hydrogel membranes, Polym. Degrad. Stab. 92 (2007) 1072–1081. https://www.sciencedirect.com/science/article/pii/S0141391007000699 (accessed October 11, 2021).

[44] I. Corazzari, R. Nisticò, F. Turci, M. Faga, Advanced physico-chemical characterization of chitosan by means of TGA coupled on-line with FTIR and GCMS: Thermal degradation and water adsorption , Polym. Degrad. Stab. 112 (2015) 1–9.

https://www.sciencedirect.com/science/article/pii/S014139101400439X (accessed October 11, 2021).

[45] D. Mudgil, S. Barak, B. Khatkar, X-ray diffraction, IR spectroscopy and thermal characterization of partially hydrolyzed guar gum, Int. J. Biol. Macromol. 50 (2012) 1035–1039. https://www.sciencedirect.com/science/article/pii/S0141813012000967 (accessed October 12, 2021).

[46] A. Paulino, J. Simionato, J. Garcia, J. Nozaki, Characterization of chitosan and chitin produced from silkworm crysalides, Carbohydr. Polym. 64 (2006) 98–103. https://www.sciencedirect.com/science/article/pii/S0144861705005412 (accessed October 12, 2021).

[47] P. Kaur, A. Choudhary, R. Thakur, Synthesis of chitosan-silver nanocomposites and their antibacterial activity, Int. J. Sci. Eng. Res. 4 (2013) 869–872. https://www.researchgate.net/profile/Rajesh-Thakur-3/publication/273455396_Synthesis_of_Chitosan-silver_nanocomposites_and_their_antibacterial_activity/links/5502edc00cf231de076fc869/Synthesis-of-Chitosan-silver-nanocomposites-and-their-antibacterial-acti (accessed October 12, 2021).

[48] E. Ferrage, G. Seine, … A.G.-E. journal, undefined 2006, Structure of the {001} talc surface as seen by atomic force microscopy: comparison with X-ray and electron diffraction results, Pubs.Geoscienceworld.Org–483 (2006) 18 . 491. https://doi.org/10.1127/0935.

[49] T. Kogure, J. Kameda, T Matsui, Stacking structure in disordered talc: Interpretation of its X-ray diffraction pattern by using pattern simulation and high-resolution transmission electron microscopy, Am. Mineral. 91 (2006) 1363–1370. https://doi.org/10.2138/am.2006.2196.

[50] D. Bilba, G. Moroi, N. Bilba, Copper (II) and mercury (II) retention properties of a polyacrylamidoxime chelating fiber, Environ. Eng. Manag. J. 5 (2006) 297–305. http://www.eemj.icpm.tuiasi.ro/pdfs/vol7/no3/4_Doina_Bilba.pdf (accessed October 12, 2021).

[51] J. Yang, S. Han, L. Yang, H Zheng, Synthesis of beta-cyclodextrin-grafted-alginate and its application for removing methylene blue from water solution, J. Chem. Technol. Biotechnol. 91 (2016) 618–623. https://doi.org/10.1002/jctb.4612.

[52] A. Paulino, M. Guilherme, A. Reis, G.M. Campese, & Muniz, E. C., J. Nozaki, Removal of methylene blue dye from an aqueous media using superabsorbent hydrogel supported on modified polysaccharide, J. Colloid Interface Sci. 301 (2006) 55–62. https://www.sciencedirect.com/science/article/pii/S002197970600333X (accessed October 12, 2021).

[53] Y. Zhou, S. Fu, H. Liu, … S.Y., Removal of methylene blue dyes from wastewater using cellulose-based superadsorbent hydrogels, Polym. Eng. Sci. 51 (2011) 2417–2424. https://doi.org/10.1002/pen.22020.

[54] A. Gürses, Ç. Doğar, M. Yalçın, … M.A., The adsorption kinetics of the cationic dye, methylene blue, onto clay, J. Hazard. Mater. 131 (2006) 217–228. https://www.sciencedirect.com/science/article/pii/S0304389405005649 (accessed October 12, 2021).

[55] S. Saber-Samandari, M Gazi, Removal of Mercury (II) from Aqueous Solution using Chitosan-graft-Polyacrylamide Semi-IPN Hydrogels, Sep. Sci. Technol. 48 (2013) 1382–1390. https://doi.org/10.1080/01496395.2012.729121.

[56] X. Wang, A Wang, Adsorption Characteristics of Chitosan-g-Poly(acrylic acid)/Attapulgite Hydrogel Composite for Hg(II) Ions from Aqueous Solution, Sep. Sci. Technol. 45 (2010) 2086–2094. https://doi.org/10.1080/01496395.2010.504436.

[57] L. Zhou, Y. Wang, Z. Liu, Q Huang, Characteristics of equilibrium, kinetics studies for adsorption of Hg (II), Cu (II), and Ni (II) ions by thiourea-modified magnetic chitosan microspheres, J. Hazard. Mater. 161 (2009) 995–1002. https://www.sciencedirect.com/science/article/pii/S030438940800589X (accessed October 12, 2021).